Journal of Instrumentation

Ion backflow studies for the ALICE TPC upgrade with GEMs

PUBLISHED BY IOP PUBLISHING FOR SISSA MEDIALAB

RECEIVED: *November 5, 2013*
ACCEPTED: *February 22, 2014*
PUBLISHED: *April 17, 2014*

3rd INTERNATIONAL CONFERENCE ON MICRO PATTERN GASEOUS DETECTORS
1–6 JULY, 2013
ZARAGOZA, SPAIN

Ion backflow studies for the ALICE TPC upgrade with GEMs

M. Ball,[a,1,2] **K. Eckstein**[a,2] **and T. Gunji**[b,2]

[a] *Technische Universität München,*
Physik-Department E18, D-85748 Garching, Germany
[b] *Center for Nuclear Study, Graduate School of Science, University of Tokyo,*
7-3-1 Hongo, Bunkyo, Tokyo, Japan

E-mail: markus.ball@tum.de

ABSTRACT: The ALICE (A Large Ion Collider Experiment at CERN) collaboration plans an upgrade of the detector during the second long shutdown of the LHC, during which the interaction rate will be increased to 50 kHz for Pb-Pb collisions. This demands operation of the Time Projection Chamber (TPC) in an ungated continuous mode. A gating grid can not be used to prevent ions drifting back into the drift volume. Gas Electron Multipliers (GEM) offer intrinsic suppression of the ion backflow. To keep distortions due to space-charge at a manageable level an ion yield of 10 to 20 back drifting ions per incoming electron is required. In this manuscript, we describe the concept of ion backflow suppression with our triple GEM prototype. Within a detailed gas study, we show our lowest ion backflow values for several different gas mixtures that have been considered for the TPC upgrade. These values have been compared with detailed simulations using ANSYS and Garfield++. Within the scope of this study, a large impact of space-charges on the ion backflow has been observed. Systematic measurements over a wide range of charge densities, for different field configurations and different drift gaps have been carried out.

KEYWORDS: Particle tracking detectors (Gaseous detectors); Time projection chambers

[1] Corresponding author.
[2] For the ALICE TPC Collaboration.

doi:10.1088/1748-0221/9/04/C04025

Contents

1 Introduction

A Time Projection Chamber (TPC) [1] with its low material budget and excellent pattern recognition capabilities, is an ideal device for three-dimensional tracking and identification of charged particles. They are used in many running experiments, including STAR [2] and ALICE [3]. In standard TPCs, Multiwire Proportional Chambers (MWPCs) [4] are used as gas amplification stages. To prevent ions produced in the avalanche from drifting back into the active volume of the TPC, gating grids are employed. This introduces a dead time, limiting the rate to $\mathcal{O}$(kHz).

The ALICE TPC is the largest TPC with an overall active volume of about 90 m^3. It employs a cylindrical field cage with a central cathode and a readout plane at each end plate. It covers full azimuth in pseudo-rapidity less than 0.9 and provides charged-particle tracking over a wide transverse momentum range. The readout planes consists of 72 readout chambers with a total of 557,568 pads.

The ALICE collaboration plans an upgrade of the detector during the second long shutdown of the LHC to fully exploit the scientific potential of the LHC at high-rate Pb-Pb collisions. At a rate of minimum bias Pb-Pb interactions of about 50 kHz, the particle tracks of five events on average will be continuously superimposed in the drift volume of the TPC. A continuous ungated mode of operation is the only way to run the TPC in 50 kHz Pb-Pb collisions. This requires replacement

of the MWPC-based readout chambers to overcome the rate limitations of the present system. Since the TPC can not be operated at 50 kHz with a gating grid, a charge amplification scheme that provides intrinsic suppression of ions must replace the MWPC-based amplification scheme. A multi-stage Gas Electron Multiplier (GEM) [5] amplification system has been chosen to replace the existing system. The limits of a triple-GEM amplification system within the boundary conditions of the ALICE TPC has been evaluated. The impact of high space-charge densities on the ion backflow has been studied and quantified. Furthermore, the gas mixture must comply with the additional requirement of low ion backflow and fast clearance of electrons and ions, maintaining the excellent detector performance. In section 2.1 a motivation for the optimal gas choice is given. As a result of the studies Ne-CO_2-N_2 (90-10-5)[1] is established as a baseline mixture for the ALICE TPC upgrade.

2 Ion backflow suppression with a GEM

For the GEM-TPC upgrade of ALICE, it is mandatory to minimize the ion backflow as a prerequisite for continuous readout and maintenance of excellent TPC performance. GEM [5] foils as a charge amplifier are the candidate to operate a TPC in continuous readout mode. The GEM technology has been established in the last decade as a robust and well proved amplification technique for gaseous detectors with excellent results for spatial resolution, transverse and longitudinal hit separation and low ion backflow. Detectors based on GEM amplification were pioneered by the COMPASS experiment at CERN [6–9], and are now routinely used in several particle physics experiments including LHCb [10], PHENIX [11], and TOTEM [12]. New applications include the use of GEM-based detectors in KLOE-2 [13] and CMS [14]. The usage of GEM detectors as readout chambers in the ALICE TPC, however, is new with regard to several aspects:

- *Ion backflow (*IB*):* the ion backflow that can be tolerated is about 1 % at a gain of 2000 in Ne-CO_2-N_2 (90-10-5). This gain is needed to achieve a sufficient signal-to-noise ratio of 20. This requires an ion yield of 20 back drifting ions per incoming electron. Any additional reduction would reduce the corrections from space-charge distortions.

- *Discharge probability:* the electric field configuration that is needed to minimize the ion backflow is in conflict with the field configuration for minimizing the discharge probability [15]. The steeper rise of the Townsend coefficients for Ne-based gases, compared to Ar-based gases, has a high impact on the discharge probability of the system. A campaign to study the discharge behavior of the IB field configuration in Ne-based gases must be performed. Particularly, the differences between weakly and strongly ionizing particles must be taken into account.

- *Long-term behavior:* long-term operation in ALICE requires careful testing the aging properties of all materials.

Suppression of ion backflow has been the subject of intensive studies [17–22].

[1] Note that this ratio defines the relative ratio of the individual gas components to each other.

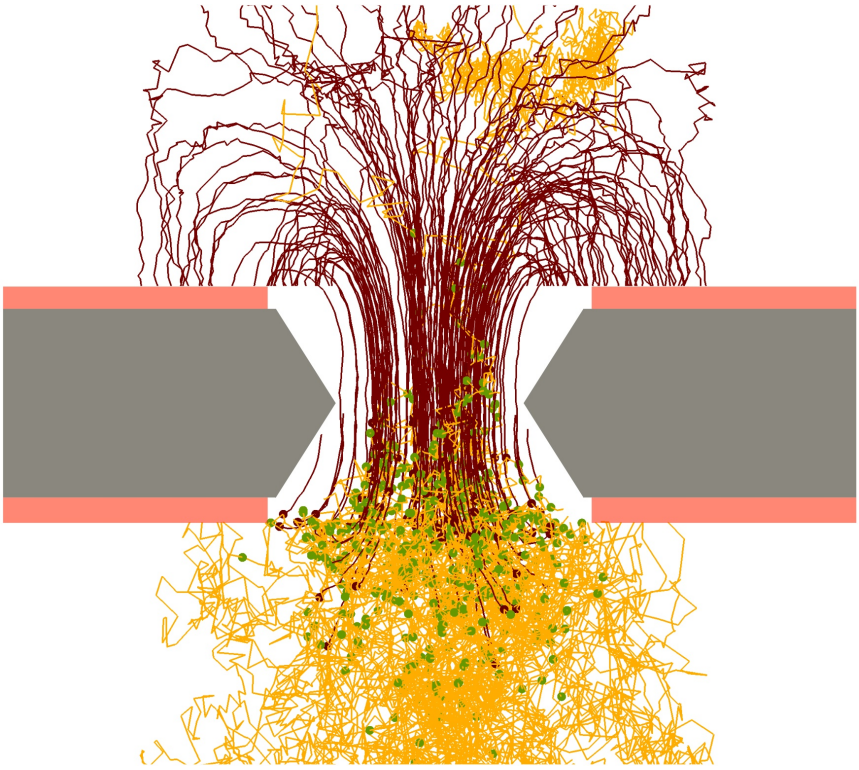

Figure 1. Garfield / Magboltz simulation of charge dynamics of two arriving electrons in a GEM hole [24]. Electron paths are shown as light lines, ion paths as dark lines. Spots mark places where ionization processes have occurred. The paths have been projected onto the cross section plane.

Figure 1 shows a simulation performed with the Garfield & Magboltz [23] packages that illustrates the suppression of ion backflow from the amplification region. Suppression is achieved by an asymmetry of the drift and extraction fields with respect to the high field inside the GEM. Ar-CO_2 gas in the ratio 70-30 has been used. Two electrons (yellow lines) are guided into the GEM hole by the drift field (here 250 Vcm^{-1}) and produce avalanches by ionizing gas molecules (brown dots). The ions created in the avalanches (dark lines) closely follow the electric field lines because of their low diffusion. Most of the ions are collected on the top side of the GEM foil, because the field inside the GEM hole is much higher than the field above the hole. Only a small number of ions re-enter the drift volume. The extraction of avalanche electrons from the hole is more efficient since the ratio of the extraction field to the field inside the GEM is typically about an order of magnitude larger (here: 3.75 kVcm^{-1}) than the ratio of the drift field to the GEM field. Therefore a small drift field to get a maximal ion collection and a high extraction field to maximally extract the electrons is favored. The fact that the charge avalanche is produced in the lower part of the hole also benefits the better extraction of electrons.

The electrons can then be transferred to another amplification stage or collected at the anode. Typically three or four GEM foils are combined in a stack. The field configuration to suppress the ion backflow for a triple GEM stack has been developed within the community of the International Linear Collider (ILC) [16]. E_{T1} and E_{ind} are chosen as high as possible. A high E_{T1} allows high extraction after the first amplification stage. E_{T2} is chosen as low as possible to achieve maximum

blocking of the ions produced at GEM3. E_{ind} is high to get the maximal and fastest signal on the readout electrode. The potential differences across the three GEMs follow an increasing order, such that $\Delta U_{\mathrm{GEM1}} < \Delta U_{\mathrm{GEM2}} < \Delta U_{\mathrm{GEM3}}$. The field configuration used in this paper follows the same idea to produce the highest amplification and the best ion blocking.

The effective gain of a GEM detector is determined by measuring the current at the readout anode I_{anode} for a given rate $R_{\mathrm{X-ray}}$ of incident X-rays coming from an ^{55}Fe-source. Each X-ray conversion produces n_{prim}[2] ionization electrons:

$$G_{\mathrm{eff}} = \frac{I_{\mathrm{anode}}}{e \cdot n_{\mathrm{prim}} \cdot R_{\mathrm{X-ray}}} \quad . \tag{2.1}$$

Defined in this way, equation (2.1) corresponds to the gain seen by the readout and takes into account charge losses in the GEM structures. A triple GEM system is leading to effective gains of the order of $10^3 - 10^4$. We define the ion backflow[3] as the ratio of cathode to anode current,

$$\mathrm{IB} = \frac{I_{\mathrm{cathode}}}{I_{\mathrm{anode}}} = \frac{\varepsilon + 1}{G_{\mathrm{eff}}} \quad , \tag{2.2}$$

where ε is the number of back drifting ions per incoming electron coming from the amplification region. Note that ion backflow also includes a contribution from ions created during the primary ionization process.

To quantify the effect of ion backflow in terms of resulting space-charge distortions one can study the gas-dependent parameters as a function of the space-charge density. The space-charge density is given as

$$\rho = \frac{\langle N_{\mathrm{ch}} \rangle_{MB} \cdot R_{MB} \cdot (\varepsilon + 1) \cdot n_{\mathrm{prim}} \cdot \mathrm{e}}{2 \cdot \pi \cdot \mathrm{r} \cdot v_{\mathrm{ion}}}, \tag{2.3}$$

with n_{prim} the number of primary charges, ε the number of back drifting ions per incoming electron and v_{ion} the ion drift velocity. These are the parameters that directly depend on the gas. $\langle N_{\mathrm{ch}} \rangle_{MB}$ the number of particles per pseudo rapidity bin, r the radial position, and R_{MB} the event rate are parameters that do not depend on the gas composition, but are determined by the experiment and detector properties. Considering only the gas dependent parameters $\rho \sim \frac{(\varepsilon+1) \cdot n_{\mathrm{prim}}}{v_{\mathrm{ion}}}$ one can compare the production of space charges as a function of different gas mixtures. However, a low space charge production is not the only requirement on a certain gas. Therefore the right choice of gas is discussed in the following.

2.1 Gas choice

The current ALICE TPC, which employs MWPCs as readout chambers, uses Ne-CO_2 (90-10) as the operating gas mixture. The addition of 5% N_2 has been tried in the past. Adding N_2 into the mixture would be beneficial as it only slightly modifies the established properties (see table 1) of Ne-CO_2 (90-10). This allowed to employ the same readout electronic. This might be an even more important argument in the future. In case a higher stability is needed due to the high rate, small

[2] In this case n_{prim} has to be modified according the true weight of the spectral distribution. This means n_{prim} should be read as $\overline{n}_{\mathrm{prim}}$.

[3] There appear different definitions of the term ion backflow in the literature. We choose this definition since it can be easily measured.

Table 1. Properties of various mixtures that could be used in modern TPCs: drift velocity v_d, and longitudinal and transverse diffusion coefficients, D_L and D_T, evaluated at 400 V/cm; $\omega\tau$ factor; effective ionization energy W_i; number of primary electrons per MIP N_p; and total number of electrons per MIP N_t.

Gas	v_d (cm/μs)	D_L ($\sqrt{\text{cm}}$)	D_T ($\sqrt{\text{cm}}$)	$\omega\tau$	W_i (eV)	N_p (cm^{-1})	N_t (cm^{-1})
Ne-CO_2-N_2 (90-10-5)	2.58	0.0221	0.0209	0.32	37.3	14.0	36.1
Ne-CO_2 (90-10)	2.73	0.0231	0.0208	0.34	38.1	13.3	36.8
Ne-CF_4 (90-10)	8.02	0.0152	0.0131	1.77	37.7	15.7	42.7
Ne-CF_4 (80-20)	8.41	0.0131	0.0111	1.84	37.3	20.5	54.1
Ar-CO_2 (90-10)	3.31	0.0262	0.0221	0.43	28.8	26.4	74.8

changes of the N_2 contribution would not require a change of the front end electronic. Also the replacement of Ne by Ar has been considered as a more drastic solution. Both solutions either using Ne-CO_2-N_2 (90-10-5) or switching to Ar-CO_2 (90-10) would resolve discharge problems resulting from a higher Townsend coefficient. As the event rate is increased about a factor of 100 operation stability is one mandatory requirement for the TPC upgrade.

Mitigating the space-charge distortions expected in the upgrade scenario is an important criterion for the gas choice. The mobility of Ar^+ ions in Ar is $1.52\,\text{cm}^2\text{V}^{-1}\text{s}^{-1}$, about three times lower than that of Ne^+ ions in Ne, $4.08\,\text{cm}^2\text{V}^{-1}\text{s}^{-1}$. We disregard here the effect of drifting CO_2^+ ions in these mixtures. Since the ion backflow is similar for these two noble gases (see section 5.1), the different mobilities result in larger space-charge distortions in argon, even at a factor of 2 lower gain (see equation (2.3)). CF_4, which provides a very high drift velocity and thus results in a reduced event pileup, is to be thoroughly validated for compatibility with all materials of the detector and the gas system, before it could be be regarded as a suitable operating gas. A set of basic properties of relevant gas mixtures is summarized in table 1.

In the anticipated configuration of our GEM system, large transfer fields are used. However, at field strengths around 4 kV/cm amplification starts in Ne-CO_2, as shown in figure 2. This limits the values that can be used for the extraction fields and therefore the ion backflow performance (see section 5.1), adding to the instability of the Ne-CO_2 mixture discussed above. An increased concentration of CO_2 rapidly decreases the drift velocity unless the field cage voltage is increased beyond its certified limits. The addition of N_2 alleviates both issues as shown in the figure and explained in [3]. Considering the main requirements as operational stability resulting from a low Townsend coefficient and low space charge production which favors a gas with high ion mobility Ne-CO_2-N_2 (90-10-5) has been chosen as default gas mixture.

We investigate whether with a conventional triple GEM system the minimum value of 20 for ε can be achieved. Several Ne-based gases and one Ar-based mixture were compared to identify the best gas choice with respect to ion suppression. The outcome of this study is presented and discussed in section 5.

3 The triple GEM setups

Our triple GEM detector was specifically built to measure ion backflow. Its most important properties can be found in table 2.

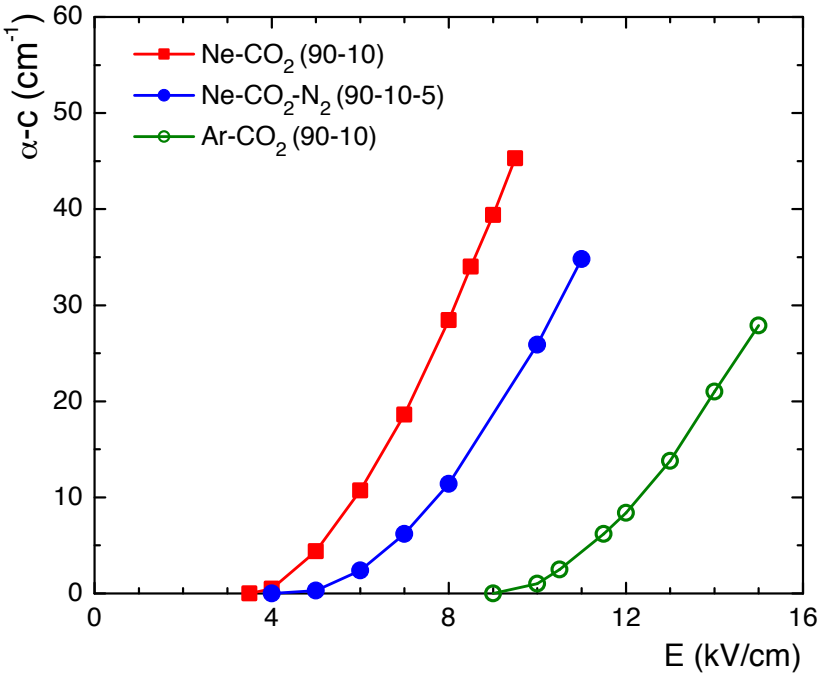

Figure 2. Difference between the Townsend and attachment coefficients in Ne-CO_2 (90-10), Ne-CO_2-N_2 (90-10-5) and Ar-CO_2 (90-10) mixtures as a function of the electric field strength. The onset of gain is shifted upwards by 1 kV/cm with the admixture of N_2 to the neon mixture. The onset for argon is substantially further away.

Table 2. Properties of the detectors with short and large drift gap.

Parameters	Short drift gap	Long drift gap
Drift gap	3 mm	80 mm
Transfer gap 1	2 mm	2 mm
Transfer gap 2	2 mm	2 mm
Induction gap	1.5 mm	3 mm
Field cage	no	yes
picoammeters	8	2

3.1 Short drift gap detector

The detector features a short drift length, individual control of each HV electrode, and the possibility to irradiate the detector from the top and the side wall. All measurements have been performed with a triple 10×10 cm^2 GEM stack. The holes have a pitch of 140 μm, an outer hole diameter of 70 μm, and an inner hole diameter of 50 μm. The distances between GEM planes and between GEM and readout can be found in table 2.

The readout consists of 512 strips that can be either read out individually or connected via analog summation cards to a total of 16 channels. By setting the appropriate jumper, one can select the corresponding size of the readout area, while all other strips remain grounded.

The picoammeters used to measure all currents are decoupled from the electric power to operate them at high voltages up to 5 kV. This requires a separate power consumption, which is realized

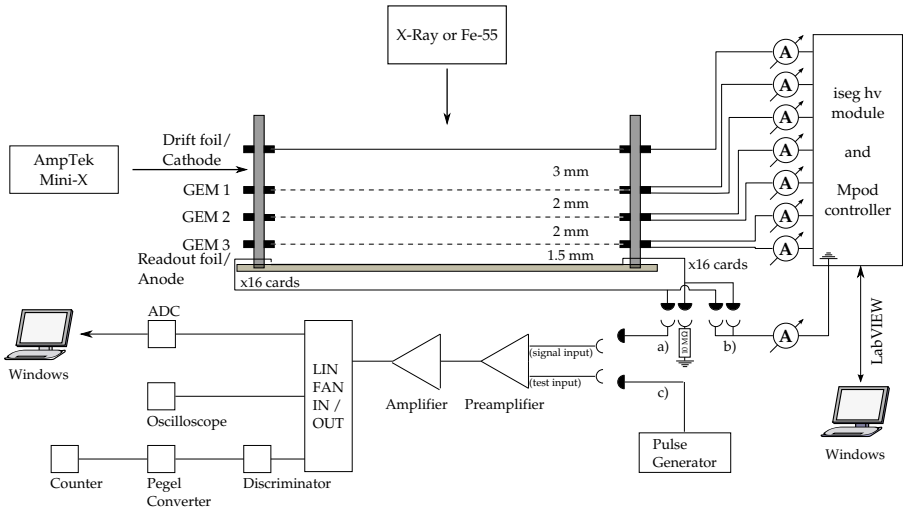

Figure 3. Sketch of the triple-GEM setup with short drift distance.

by two 9 V batteries. The picoammeters are kept at a floating potential. They are able to measure currents to less than 100 pA level are sampled with a 16 bit ADC. The data is sent out to a wireless receiver, connected to a readout PC. However, for measurements below 100 pA, the picoammeters must be in a shielded environment, otherwise external noise strongly influence the measurement.

The chamber has seven high voltage connectors that can be powered individually. To measure the current of each channel, one picoammeter is connected at each electrode (see sketch of the detector setup in figure 3). The readout chain can also be realized with conventional spectroscopy amplifiers and a multichannel analyzer for recording pulse height spectra. A small X-ray tube[4] with a gold target is used to irradiate the detector. The spectrum peaks at the L_α (9.5 keV), L_β (12 keV), and the L_γ (14 keV) lines. A non negligible background comes from Bremsstrahlung photons. The X-ray voltage is set to minimize the effect of these Bremsstrahlung photons. However, as the gain determination has been done with an ^{55}Fe-source, the X-ray tube is only used to produce high currents, that are well above the 100 pA level of the picoammeter. This way influences such as noise or small offsets of the devices can be neglected.

The ion backflow parameter and ε used in the following are defined according to equation (2.2). The gain is determined according equation (2.1) by recording the current at the pad plane and the rate of absorbed X-rays of known energy.

3.2 Long drift gap detector

The detector housing used for ion backflow measurement at CERN comprises a GEM holder and a field cage. The GEM box is equipped with HV feedthroughs for up to four 10×10 cm^2 foils and a pad plane subdivided into 16×16 pads. All pads are connected together for measurement of the current. The field cage, constructed from Rohacell to allow for easy irradiation with X-rays, is 8 cm deep and has a drift electrode and 10 strips made of copper. The drift electrode is powered by one channel of a HV power supply, and its current is measured with a floating picoammeter with

[4] An Amptex Mini-X with a gold transmission target has been used (see specifications www.amptek.com/minix.html).

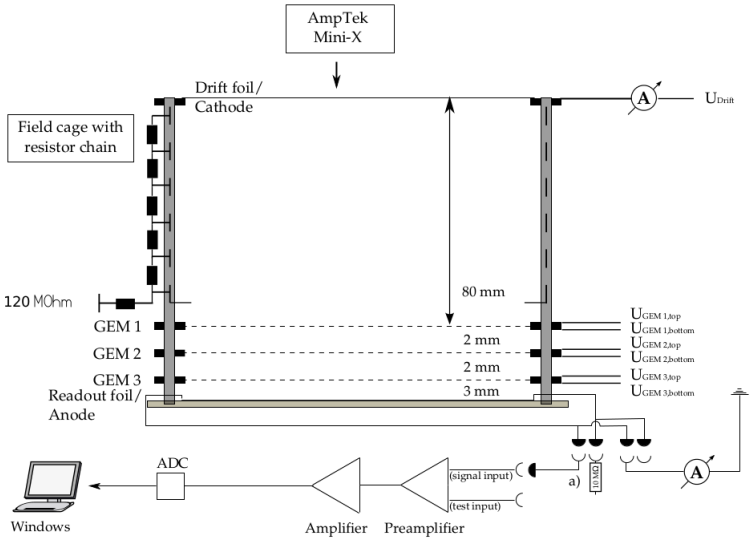

Figure 4. Sketch of the triple-GEM setup with long drift distance.

100 pA resolution. The field cage is powered by a different HV channel so that the current through its ten 10 MΩ resistors does not add to the small current on the drift electrode. Finally, an external resistor ensures reasonable matching of potentials of the last strip and the top GEM electrode. For a triple GEM stack, this value is 120 MΩ. The gas is supplied from a premixed bottle for the reference measurements with Ar-CO_2 (70-30) and from a mixer for the other gas mixtures. The HV is supplied by programmable CAEN N1471A power supplies with RS232 interfaces to a PC running a custom-written Labview application. This program allows for parallel ramping up and down of the GEM and drift voltages in order to efficiently perform voltage scans. An X-ray[5] tube is used as a source of radiation. Here the spectrum peaks at the K_α (22 keV) and the K_β (25.5 keV). A sketch of the detector with large drift gap can be found in figure 4. For the measurements of section 4.2 two drift distances have been used. A long drift gap of 80 mm with a field cage and a resistor chain and a short drift gap of 3 mm without a field cage and without a resistor chain. This way the impact of the drift gap and space-charge on the IB could be studied

4 Rate dependence of the ion backflow

A strong systematic effect on the ion backflow has been discovered within the scope of this study. The ion backflow has been measured for different field configurations, X-ray rates, gain and drift length. It should be noted that this rate effect is not related to the drop of gain and efficicency according to the rate capability of GEMs. It is related to a change of the local electric field due to high ion space-charge density in front of the GEMs that mainly affects the ions but not the electrons.

[5] An Amptex Mini-X with a silver transmission target has been used (see specifications www.amptek.com/minix.html).

Table 3. Field configuration for the charge density scans for Ar-CO_2 (90-10) and Ne-CO_2-N_2 (90-10-5)

Field Configuration	Ar-CO_2 (90-10)	Ne-CO_2-N_2 (90-10-5)
ΔU_{GEM1} (V)	285	250
ΔU_{GEM2} (V)	320	280
ΔU_{GEM3} (V)	360	325
E_{drift} (kV/cm)	0.4	0.4
E_{T1} (kV/cm)	5.0	5.0
E_{T2} (kV/cm)	0.2	0.2
E_{ind} (kV/cm)	4.5	4.5

When the uniform ion density is assumed in the drift space, the electric field is charged as follows due to the existence of the space-charge density

$$E(z) \sim E_{\mathrm{d}} - \frac{\rho \cdot d}{2 \cdot \epsilon_0} + \frac{\rho \cdot z}{\epsilon_0} \tag{4.1}$$

where E_{d} is the drift field, ρ denotes the space-charge density, d is the drift length of the system, ϵ_0 the permittivity, and z the distance from the top of the GEM1. If the space-charge density is comparable to $\frac{\rho \cdot d}{2 \cdot \epsilon_0} \sim E_{\mathrm{d}}$ a substantial reduction of the ion backflow is expected. The term $\frac{\rho \cdot z}{\epsilon_0}$ is negligible as only the local drift field modification above the GEM hole has an impact on the ion backflow, where z is close to zero. Detailed measurements have been conducted to verify the space-charge effect of the ion backflow.

4.1 Measurements with the short drift gap detector

The rate dependence of the ion backflow has been measured with a short drift gap detector to verify that the measurements described in section 5 are not biased by the space-charge density of ions. The profile of the X-ray spot has been estimated by measuring the currents on groups of adjacent strips. A beam ellipse with the semi-axes $\sigma_{\mathrm{x}} = 7.2$ mm and $\sigma_{\mathrm{y}} = 9.5$ mm has been determined. This leads to beam spot sizes of $A_{\pm 1\sigma} = 2.14\,\mathrm{cm}^2$ and $A_{\pm 2\sigma} = 8.54\,\mathrm{cm}^2$. The following results are based on the estimated spot size $A_{\pm 1\sigma}$.

Ar-CO_2(90-10) and Ne-CO_2-N_2 (90-10-5) gas mixtures and a drift length of 3 mm have been used to cross check if the measured ion backflow is biased by space-charge effects.

The ion backflow as a function of ρ_{ion} is given in figure 5 for the field configurations given in table 3. For charge densities beyond $10^3\,\mathrm{fC/cm}^3$ the ion backflow is affected by space-charge. Therefore, the measurements in section 5 have been done for an X-ray current of $5\,\mu$A and an X-ray voltage of 30 kV, which according to equation (4.2), corresponds to charge densities of about $200\,\mathrm{fC/cm}^3$ for Ne-CO_2-N_2 (90-10-5) and about $1000\,\mathrm{fC/cm}^3$ Ar-CO_2(90-10). These charge densities are of the same order as the ones expected in the upgrade scenario and do not affect the ion backflow.

4.2 Measurements with the long drift gap detector

In the measurements with the long drift gap detector, it was also observed that the ion backflow strongly depends on the X-ray rate and the drift length, as shown in figure 6. The field configuration

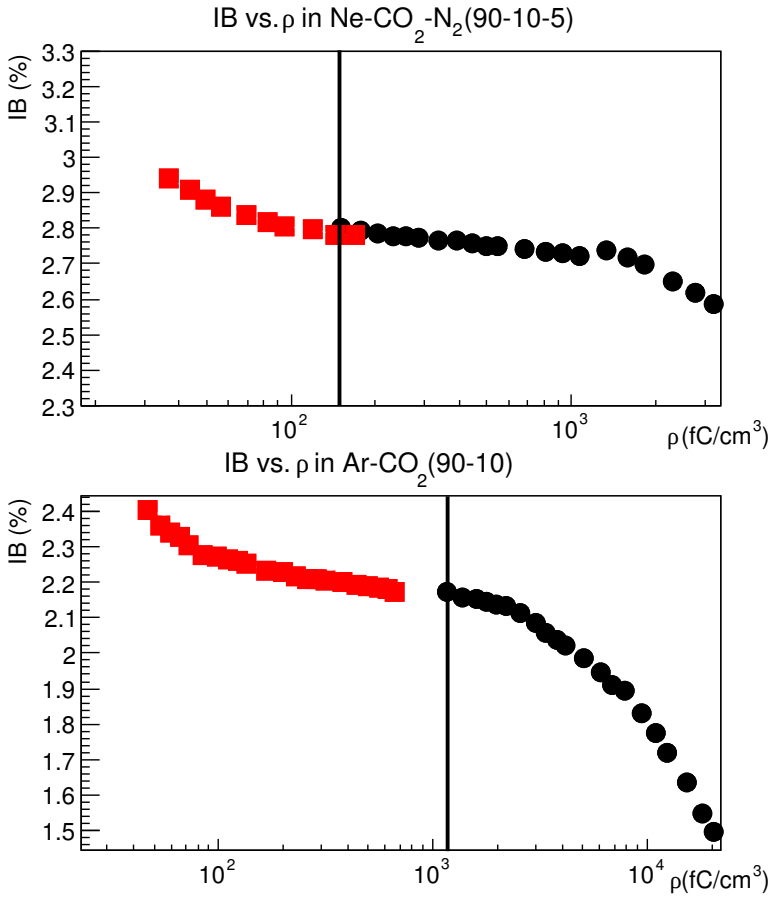

Figure 5. IB as a function of the space-charge density with the drift length fixed to 3 mm. The black dots show a range of 130 μA to 5 μA X-ray current at an X-ray voltage of 30 kV. The red dots indicate the behavior when a 1 cm aluminum absorber has been placed in front of the X-ray tube. The black line indicates the current of the X-ray tube and the corresponding charge density that has been used for the field scans of section 5.1. For both gas mixtures no bias of the ion backflow is expected at this point.

for this setup is given in table 4. The left panel of figure 6 shows IB in 3 mm and 80 mm drift lengths as a function of the current on the readout pad, which is given according to equation (2.1) as $G_{\text{eff}} \cdot n_{\text{prim}} \cdot e \cdot R_{\text{X-ray}}$. As mentioned in the section 3.2 the space-charge behavior of the triple GEM system has been measured for two different drift length. In these measurements, all potentials are kept constant, and the increase in current on the pad is due to the increase of the X-ray rate. At the same current, significantly different results of the ion backflow have been observed for the 3 mm and 80 mm drift length.

The right panel of figure 6 shows IB as a function of the space-charge density multiplied by the drift length d for the case of a 3 mm (closed) and a 80 mm drift space (open) i.e. the total charge per unit area in the drift volume. The space-charge density in the drift volume is estimated by

$$\rho = \frac{I_{\text{drift}}}{A \cdot v_{\text{ion}}} \tag{4.2}$$

where I_{drift} is the current measured at the drift electrode, A the area covered by the X-ray beam profile, and v_{ion} the drift velocity of ions for the given electric drift field in a gas mixture. The

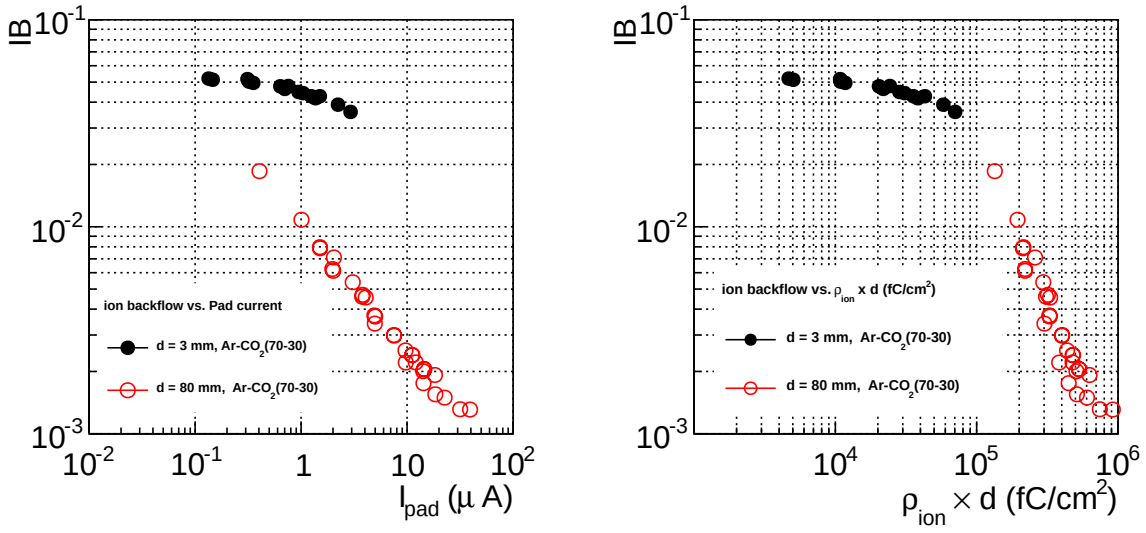

Figure 6. Left: IB as a function of the current on the readout pad. Open and closed symbols correspond to the results for the 80 mm and 3 mm drift spaces, respectively. Right: the ion backflow as a function of ρ_{ion} multiplied by d.

Table 4. Field configuration for the charge density scan with the large drift gap detector for Ar-CO_2 (70-30)

Field Configuration	Ar-CO_2 (70-30)
ΔU_{GEM1} (V)	360
ΔU_{GEM2} (V)	360
ΔU_{GEM3} (V)	360
E_{drift} (kV/cm)	0.4
E_{T1} (kV/cm)	3.0
E_{T2} (kV/cm)	3.5
E_{ind} (kV/cm)	5.0

ion drift velocity of argon based mixtures at 400 V/cm is about v_{ion} = 600 cm/s and for neon it is v_{ion} = 1600 cm/s. The diameter of the X-ray irradiation spot at the pad plane was measured with a photographic paper to be 1 cm.

The dependence of the ion backflow on $\rho \times d$ has been confirmed by the measurements with a single standard GEM. The reason to switch to a single GEM was to simplify the GEM amplification system. This way space-charge effects between the different transfer regions can be excluded. The left panel of figure 7 shows IB as a function of the gain for a single standard GEM in Ar-CO_2 (70-30) and Ne-CO_2 (90-10). The drift lengths in the measurements is 3 mm or 19 mm and the X-ray rate ($R_{\mathrm{X-ray}}$) is kept constant during the measurements.

The right panel of figure 7 shows IB as a function of $\rho \times d$. The spot of the X-ray is estimated from the size of the collimator (8 mm). It is clearly seen that the ion backflow strongly decreases when $\rho \times d$ exceeds a few 10^4 fC/cm^2.

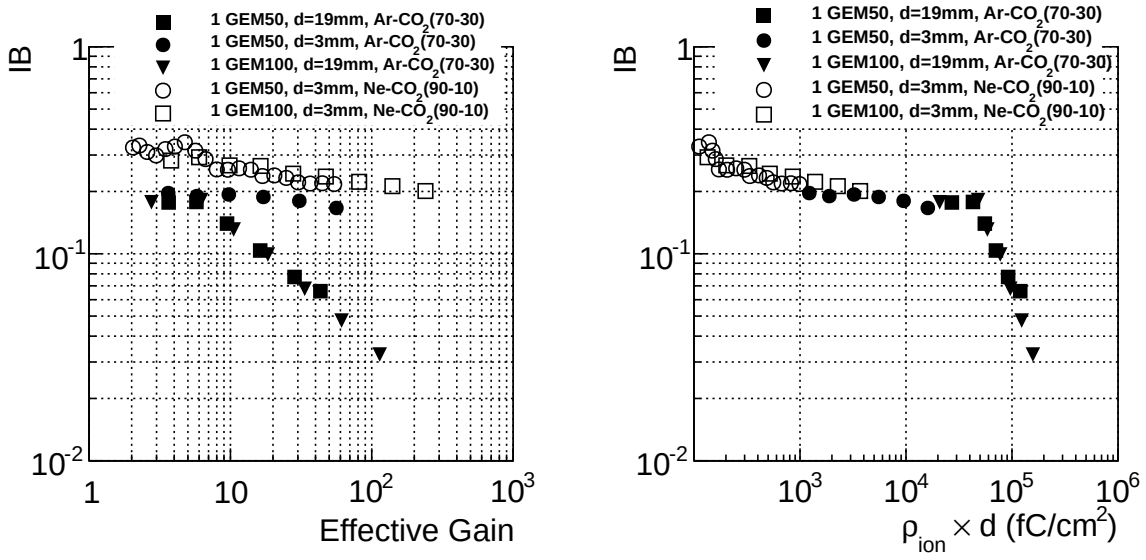

Figure 7. Left: IB as a function of the gain for a single standard GEM in Ar-CO_2 (70-30) and Ne-CO_2 (90-10). Right: IB as a function of $\rho_{\text{ion}} \times d$ in Ar-CO_2 (70-30) and Ne-CO_2 (90-10) for the same foil.

4.3 Comparison of the results

The results of the previous section show that the values for ion backflow can be severely biased by a high charge density and have been observed for both detector setups independently. However the onset value of the rate-dependent effect is not in quantitative agreement. In figure 6 the onset starts at a $\rho \times d$ of $4{\cdot}10^4$ fC/cm^2 in the large drift gap detector. In the case of the short drift gap detector, as shown in figure 5 the onset starts at about $6{\cdot}10^2$ fC/cm^2. Note that figure 5 is shows the IB as a funtion of ρ. To compare the results the value has to be multiplied with the 3 mm drift gap. The decrease of ion backflow as a function of ρ (see figure 5) has been assumed to about $2{\cdot}10^3$ fC/cm^3. This strong discrepancy is not yet fully understood. There are three possible explanations, that must be further investigated. The biggest impact can be assumed from the different electric field configuration that has been used for the both detectors. The space-charge density strongly depends on the ion mobility. E_{T2} differs significantly, but also ΔU_{GEM} for all GEMs is very different for the two detectors. This means that for the large gap detector all GEMs contribute to the space charge with a dominant contribution from GEM3. In the small drift gap detector, with its low E_{T2} and increasing ΔU_{GEM} the dominant contribution to the space-charge comes from the first two GEM foils.

A minor contribution results from the different gas mixtures. For the long drift gap detector Ar-CO_2 (70-30) has been used; for the short drift gap detector Ar-CO_2 (90-10) and Ne-CO_2-N_2 (90-10-5) have been used. The ion mobility changes about 15 % changing the gas composition from Ar-CO_2 (90-10) to Ar-CO_2 (70-30). As v_{ion} is directly entering equation (4.2) this effect has to be taken into account. However, it is clear that this difference alone can not explain the two orders of magnitude difference between the results.

A third point concerns the beam profile of the two systems. For the short drift gap detector the beam profile has been measured to be non-uniform. The beam profile of the long drift gap

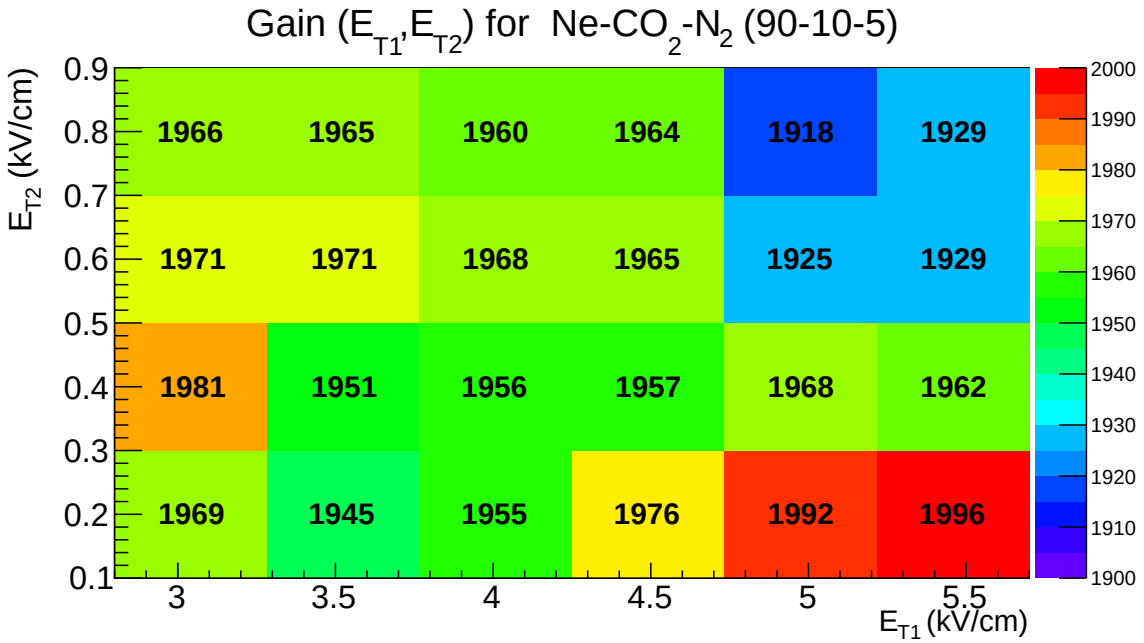

Figure 8. Gain normalization for the scan of E_{T1} and E_{T2} in Ne-CO_2-N_2 (90-10-5). To keep the effective gain at the readout constant, ΔU_{GEM3} was modified accordingly.

detector has been measured with a Polaroid and assumed to be uniform. Since X-ray tube from the same distributor were used, a non uniform beam (as shown in section 4.1) profile seems more appropriate. These three effects must be unified in upcoming measurements to achieve quantitative agreement.

However, already these results show, that the values for ion backflow can be severely biased by high charge densities and that the drift length plays an important role for the extrapolation of the results.

5 Ion backflow results for a triple GEM system

5.1 Measurements with a triple GEM system

With the triple GEM detector setup described in section 3.1 an extensive gas study has been performed. The goal was to compare the different gas mixtures with respect to their ion backflow behavior. Measurements were made with an X-ray tube. The X-ray current was minimized to 5 μA to avoid space-charge effects.

To find the optimal ion backflow settings, the transfer fields E_{T1} and E_{T2} were systematically scanned while the voltage across GEM3 was varied to keep the gain at the desired value. The effective gain was kept at a level of $\sim$2000 for neon mixtures and $\sim$1000 for argon. The goal was to compare the gases at the same signal-to-noise ratio because argon yields two-times more primary electrons for minimal ionizing particles.

The specific electric field configuration for each of the gases is given in table 6. Figure 8 shows an example of the gain dependence on E_{T1} and E_{T2} for Ne-CO_2-N_2 (90-10-5). Five gas mixtures have been compared within the scope of this study. The neon based gases are Ne-CO_2 (90-10),

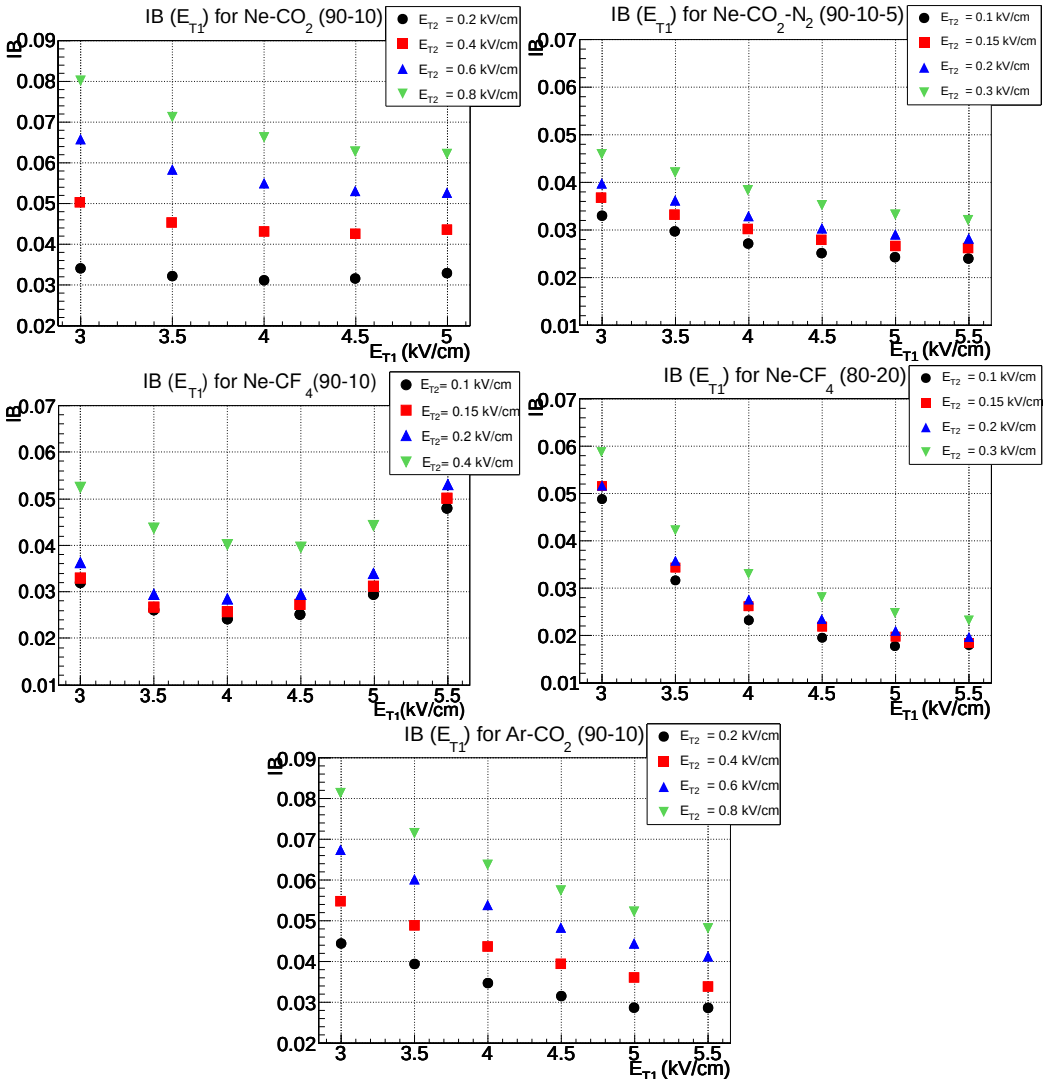

Figure 9. Measured ion backflow as a function of E_{T1} for four different settings of E_{T2} and five different gas mixtures.

Ne-CO_2-N_2 (90-10-5), Ne-CF_4 (90-10) and Ne-CF_4 (80-20). Ar-CO_2 (90-10) was the only argon based gas used. The motivation for the gas study has been discussed in section 2.1. In this section also some basic properties of the gas mixtures can be found in table 1.

In figure 9 the ion backflow is shown as a function of E_{T1} for these five gas mixtures. For Ar-CO_2 (90-10) and Ne-CO_2-N_2 (90-10-5), a clear decrease of the ion backflow as a function of E_{T1} is visible due to the higher extraction efficiency of GEM1 and higher ion blocking efficiency of GEM1 top and bottom electrode. This effect is not present for Ne-CO_2 (90-10) and Ne-CF_4 (90-10), because at transfer fields above 4 kV/cm gas amplification starts to occur. This is in agreement with figure 2 that shows the Townsend coefficient as a function of the electric field. A significant fraction of ions escapes to the drift volume, so that a high E_{T1} is no longer beneficial. This effect is very clearly visible for low values of E_{T2} because then the contribution of GEM3 to the ion backflow is minimal. Since the gain is kept constant over the whole parameter space, the same

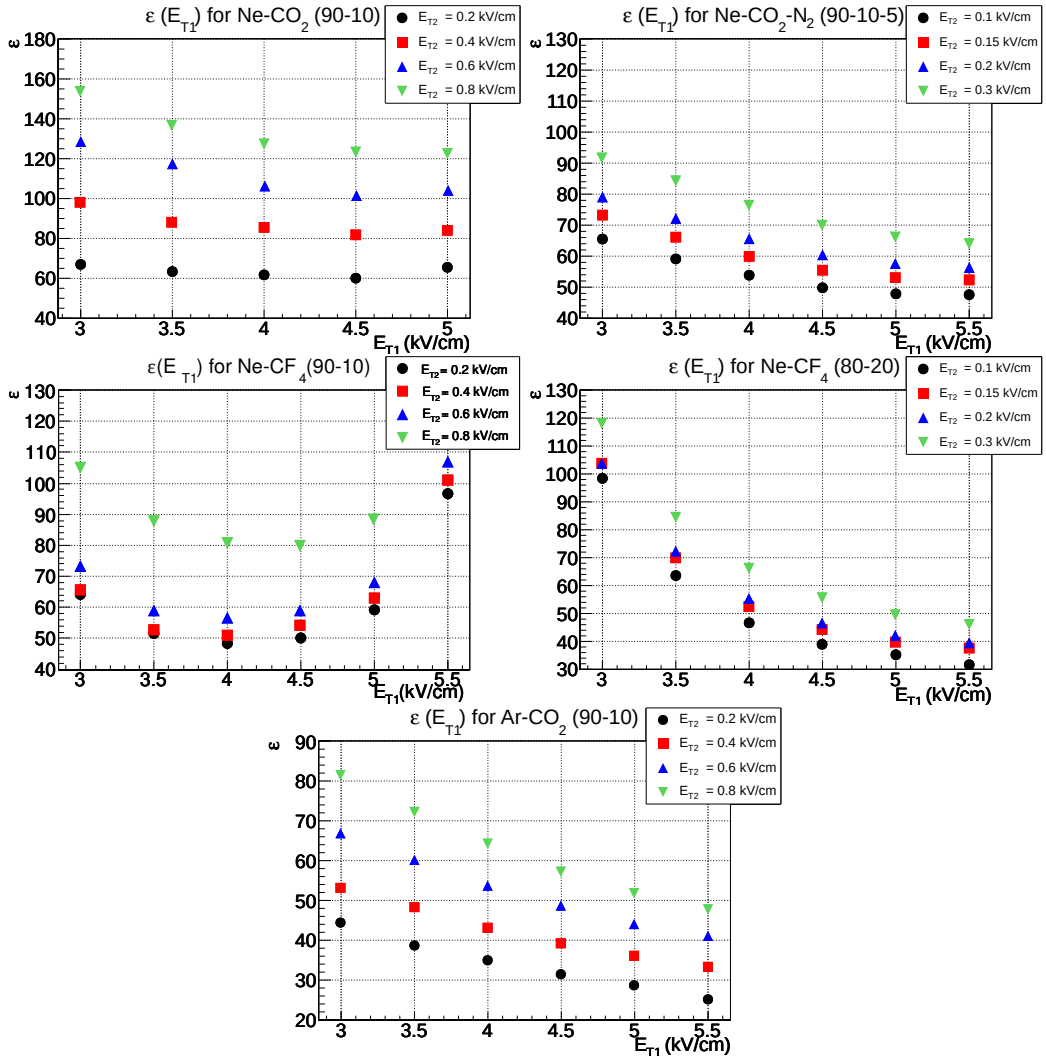

Figure 10. ε as a function of E_{T1} for four different settings of E_{T2} and five different gas mixtures.

behavior is visible in figure 10, which plots the number of back drifting ions per incoming electron, ε, as a function of E_{T1} for four different values of E_{T2}.

To determine the most promising gas candidate in terms of IB the ion backflow is compared for the E_{T1} value where the ion backflow becomes minimal. The transfer field E_{T2} is at 0.2 kV/cm for all gases. The values of this comparison can be found in table 5. The main outcome of this comparison is the relative space-charge density ρ (see equation (2.3)) which has been normalized to the space-charge density of Ne-CO_2-N_2. One can clearly see that Ar-CO_2 due to its low ion mobility would result in a 2.4 times higher space-charge density than Ne-CO_2-N_2 and would therefore be less favored with respect to space-charge distortions. The most attractive gas candidates apart from Ne-CO_2-N_2 are Ne-CF_4 (90-10) and Ne-CF_4 (80-20). For Ne-CF_4 in the ratio 90-10 and 80-20 the expected space-charge would be on a comparable level or even below the baseline mixture. However, as mentioned in section 2.1 these mixtures are to be considered only if a comprehensive material validation program is completed successfully.

Table 5. Ion backflow and ε obtained for all tested gas mixtures at their best E_{T1} and an E_{T2} = 0.2 kV/cm. Note that for Ar-CO_2 (90-10) ε is about a factor two smaller. However, taking equation (2.3) into account, the relative space-charge value is a factor 2.4 higher. The space-charge values of all values are normalized to Ne-CO_2-N_2.

Gas Mixture	Gain	IB (%)	ε	E_{T1} (kV/cm)	E_{T2} (kV/cm)	ρ(relative)
Ne-CO_2 (90-10)	1960 $\pm$ 50	3.10	61.7	4	0.2	1.096
Ne-CO_2-N_2 (90-10-5)	2000 $\pm$ 12	2.82	56.3	5.5	0.2	1
Ne-CF_4 (90-10)	2010 $\pm$ 16	2.84	56.5	4	0.2	1.004
Ne-CF_4 (80-20)	2000 $\pm$ 20	1.97	39.3	5.5	0.2	0.698
Ar-CO_2 (90-10)	990 $\pm$ 20	2.86	25.0	5.5	0.2	2.396

Table 6. Field configuration for the gases selected in for this study. All settings follow the same ion backflow characteristics.

	Ar-CO_2 (90-10)	Ne-CO_2 (90-10)	Ne-CO_2-N_2 (90-10-5)	Ne-CF_4 (90-10)	Ne-CF_4 (80-20)
ΔU_{GEM1} (V)	280	235	263	240	270
ΔU_{GEM2} (V)	315	245	305	270	300
ΔU_{GEM3} (V)	adjustable	adjustable	adjustable	adjustable	adjustable
E_{drift} (kV/cm)	0.4	0.4	0.4	0.4	0.4
E_{T1} (kV/cm)	3.0-5.5	3.0-5.0	3.0-5.5	3.0-5.0	3.0-5.5
E_{T2} (kV/cm)	0.2-0.8	0.2-0.8	0.1-0.4	0.1-0.4	0.1-0.3
E_{ind} (kV/cm)	4.5	3.8	4.0	4.0	4.0

Table 7. Lowest values of ion backflow and ε of a triple GEM system obtained for the most promising gas mixtures.

Gas Mixture	Gain	IB_{min} (%)	ε_{min}	E_{T1} (kV/cm)	E_{T2} (kV/cm)
Ne-CO_2-N_2 (90-10-5)	2000 $\pm$ 4	2.38	47 .5	5.5	0.1
Ne-CF_4 (90-10)	2005 $\pm$ 18	2.40	48.4	4	0.1
Ne-CF_4 (80-20)	2010 $\pm$ 20	1.77	35.2	5.0	0.1

The most favored gas-mixtures have been evaluated also for values of E_{T2} below 0.2 kV/cm. Due to the important role of a low transfer field E_{T2} for ion blocking, the study of the most promising gases Ne-CO_2-N_2 and Ne-CF_4 was extended to $E_{T2} = 0.1$ and 0.15 kV/cm. In figure 9 the ion backflow is shown as a function of E_{T1} for $E_{T2} = 0.1$ and 0.15 kV/cm. It should be mentioned that for the low values of E_{T2} future measurements have to prove that the detector performance such as the energy resolution can be maintained. For Ne-CO_2-N_2 (90-10-5) and Ne-CF_4 (90-10) a further reduction of the ion backflow to about 2.5 % is achieved, resulting in $\varepsilon \approx 50$. In the case of Ne-CF_4, the onset of gas amplification in the transfer gaps can be avoided by increasing the quencher concentration to 20 %. Figure 9 shows that at an effective gain of 2000 and for Ne-CF_4 (80-20) the ion backflow indeed decreases to 1.8 % ($\varepsilon = 35$) for $E_{T2} = 0.1$ kV/cm and $E_{T1} = 5.0$ kV/cm. For $E_{T1} = 5.5$ kV/cm an even lower value of $\varepsilon = 32$ has been reached. The results of these studies for

all gas-mixtures are summarized in table 7. Even these IB values exceed the specifications based on the maximum tolerable drift field distortions, so that alternatives to a conventional triple GEM system have to be explored.

5.2 Simulations of a triple GEM system

The gas gain and the ion backflow were studied with the Garfield++ simulation package [23] and compared with experimental measurements. The geometry of the detector, the material properties of the GEM, the voltage configurations, and the boundary conditions were defined in ANSYS [25]. This program calculates the electric field in the detector with a finite elements method. For the calculation of the properties of gas mixtures and transport properties of electrons in a given electric field the simulation packages Heed and Magboltz were used. All gas mixtures were simulated at room temperature and standard pressure. Electron drift and the avalanches inside a hole were studied with a microscopic transport and avalanche method. In Garfield++, this method tracks the electron path at the molecular level using the drift velocity and the diffusion, Townsend, and attachment coefficients as calculated by Magboltz from the various electron-gas cross sections. Penning effects are introduced in the calculation of the gas gain. Because a microscopic transport calculation for ions is not available in this package, transport parameters such as the ion mobility as a function of the field strength, over the gas density (E/N) are set by hand according to refs. [26–28]. Diffusion of ions is assumed to proceed according to the thermal limit. A Monte Carlo integration technique is used to track ions. The triple GEM detector configuration described in section 3 is simulated.

We found that the alignment of the holes of GEM1 and GEM2 crucially affects the resulting ion backflow for high E_{T1}. Since the hole alignment between standard GEMs cannot be controlled in the measurements, misalignment between GEM1 and GEM2 are introduced as a free parameter in the simulations. The field configurations used in the measurements and simulations in Ar-CO_2 (90-10), are summarized in table 6. The left panel of figure 11 shows IB as functions of E_{T1} and E_{T2} with a misalignment of 50.3 μm between GEM1 and GEM2. This value are used in agreement with the average misalignment assuming a random orientation of the GEM foils. The effective gas gain with this setup is 1000 in the measurements and from 850 to 1200 in simulations. The error bars represent the RMS of ion backflow. With the chosen misalignment, the measured ion backflow values are well reproduced by the simulation. The right panel of figure 11 shows the fraction of back drifting ions in the drift space from GEM3, GEM2, and GEM1 for various E_{T1} and E_{T2} settings. As E_{T2} decreases and E_{T1} increases, the number of ions drifting back into the drift region from GEM3 is reduced and the contribution of ions from GEM2 becomes relatively large. For the case of E_{T1} = 5.5 kV/cm and E_{T2} = 0.2 kV/cm, the ion backflow of 2 % is dominated by ions from GEM2, which points to the possibility of further suppression of ion backflow by tuning the gain sharing between GEMs.

The capability to describe the effective gain and the ion backflow has been checked for Ne-CO_2 (90-10), and Ne-CO_2-N_2 (90-10-5). The corresponding field configurations and GEM voltages used in the measurements and simulations are summarized in table 6. The effective gas gain with this setup is 1800 – 2400 in simulations and 2000 in the measurements. The left plot of figure 12 shows IB as functions of E_{T1} and E_{T2} with a misalignment of 45.9 μm. For a misalignment of 50.3 μm the ion backflow is overestimated by 20 %. Another consistency check has been per-

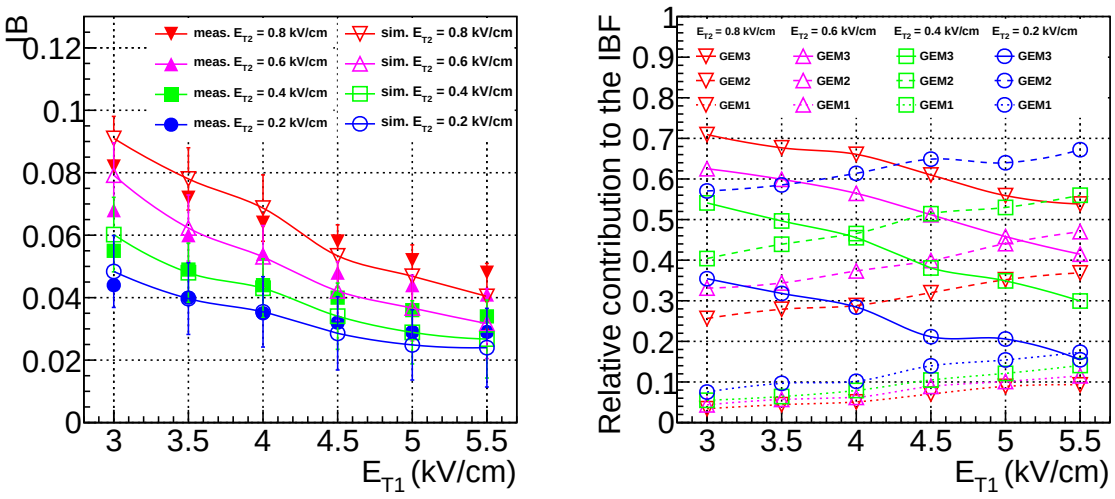

Figure 11. Left: IB as function of E_{T1} and E_{T2} from measurements (closed) and simulations (open) in Ar-CO_2 (90-10), at a gain of 1000. Right: the fraction of back drifting ions from GEM3 (solid lines), GEM2 (dashed lines), and GEM1 (dotted lines) to the total ions as a function of E_{T1} for various E_{T2} settings.

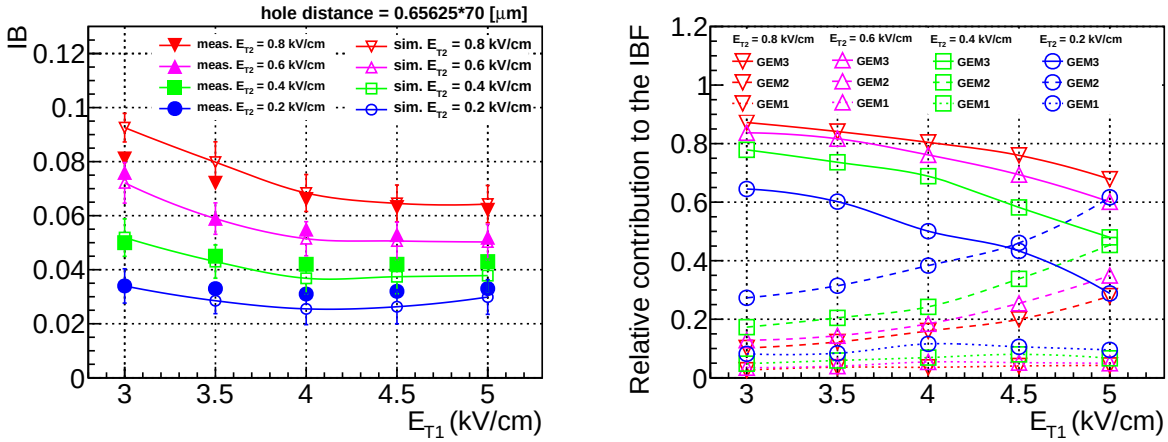

Figure 12. Left: IB as function of E_{T1} and E_{T2} from measurements (closed symbols) and simulations (open symbols) with a misalignment of 45.9 μm in Ne-CO_2 (90-10). Right: fraction of the back drifting ions from GEM1, GEM2, and GEM3 as a functions of E_{T1} and E_{T2}.

formed for Ne-CO_2-N_2 (90-10-5), for which the GEM voltages and field settings summarized in table 6 were used. Figure 13 shows IB as functions of E_{T1} and E_{T2} in Ne-CO_2-N_2 (90-10-5) for a misalignment of 45.9 μm. Although some difference in IB is observed for $E_{T2} \geq 0.7$ kV/cm and $E_{T1} \leq 3.5$ kV/cm, the measured ion backflow for $E_{T2} \leq 0.6$ kV/cm is well described by the simulations.

The left and right plots of figure 14 shows IB as a function of E_{T1} at $E_{T2} = 0.1$ kV/cm with a misalignment of 35 μm to 43.7 μm in Ne-CF_4 (90-10), and Ne-CF_4 (80-20), respectively.

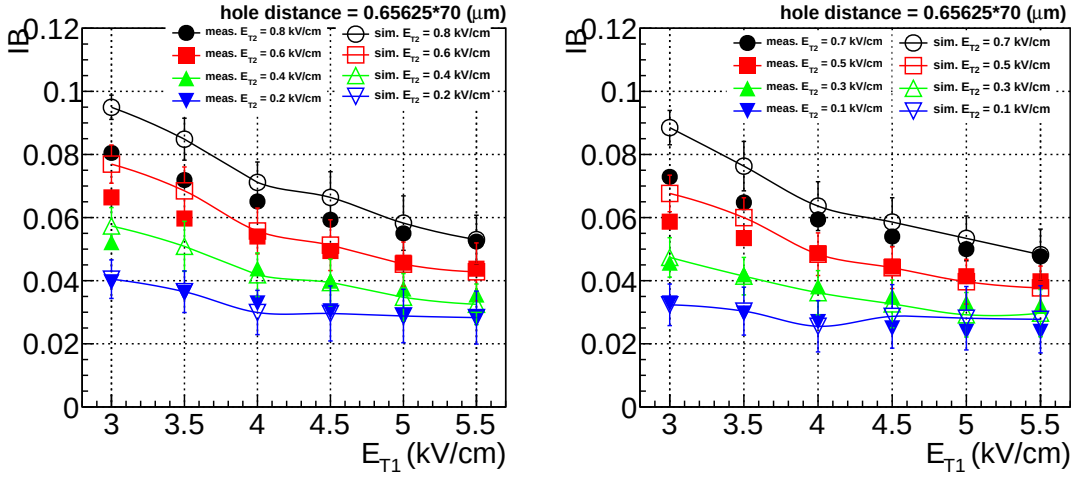

Figure 13. Left: IB as function of E_{T1} from measurements (closed symbols) and simulations (open symbols) with a misalignment of 45.9 μm in Ne-CO_2-N_2 (90-10-5) Right: IB as functions of E_{T1} from measurements (closed symbols) and simulations (open symbols) with the same misalignment.

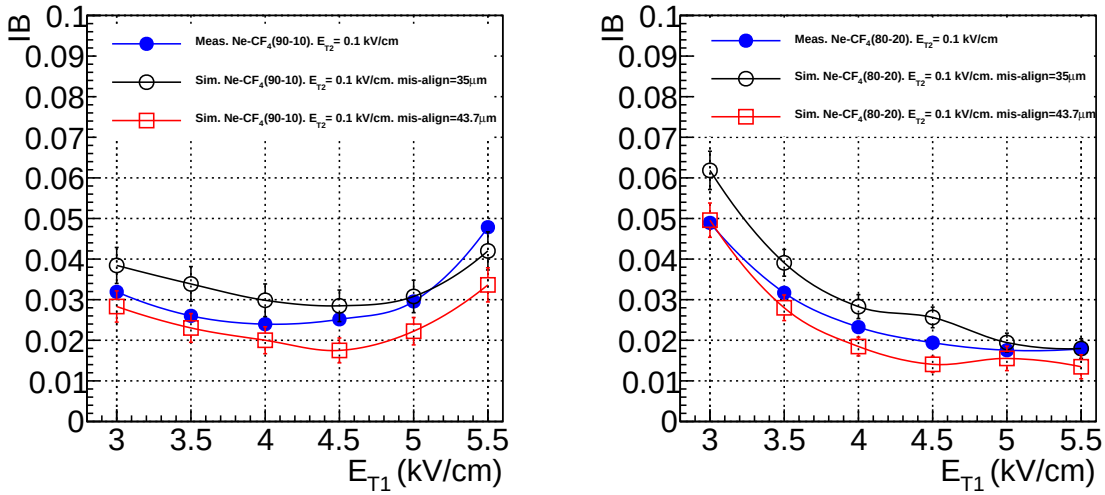

Figure 14. Left: IB as a function of E_{T1} from measurements (closed symbols) and simulations (open symbols) with a misalignment of 35 μm to 43.7 μm in Ne-CF_4 (90-10). Right: IB as a function of E_{T1} from measurements (closed symbols) and simulations (open symbols) with a misalignment of 35 μm to 43.7 μm in Ne-CF_4 (80-20).

Although the absolute agreement is still not perfect, the trend is well reproduced by simulations. However, it is unphysical for the measured ion backflow in Ar-CO_2, Ne-CO_2, Ne-CO_2-N_2, and Ne-CF_4 to be reproduced by using different misalignment. The uncertainties in the mobility, longitudinal and transverse diffusion constants of ions at low electric field strength, where no measurements exist and might contribute to this apparent discrepancy.

6 Conclusion and Outlook

A systematic study of ion backflow in small-size triple GEM prototype detectors was performed. The measurements are compared to simulations based on the Garfield++ package. In the course of these studies, the importance of the ion space-charge area density, $\rho_{\text{ion}} \times d$, in the detector was recognized. In particular, a strong impact on ion backflow is observed when the ion space-charge density is large. These observations are based on systematic variations of the irradiation rate and the drift length. Since the corresponding ion space-charge densities under ALICE running conditions are low, all quantitative studies are performed at low irradiation rates.

In triple GEM systems using standard CERN 10x10 cm^2 foils (see GEM properties in section 3.1), ion backflow values of 2–3 % are observed in different mixtures of argon and neon with CO_2 and nitrogen. These results are obtained after careful optimization of the potential settings, typically a high E_{T1} ($\sim$5 kV/cm) and low E_{T2}. The IB values exceed the specifications based on the maximum tolerable drift field distortions.

R&D activities will continue according to the outcome of this study, and will include a quadruple GEM setup, which is a very promising solution. Alternative GEM geometries such as large and small pitch foils and single conical-hole patterns will be studied.

Alternative technologies such as COBRA GEMs based on GEM technology [29] or the combination of a GEM and Micromegas have a good potential to achieve small ion backflow values. However, it will be a challenge to produce them in the size required for the ALICE TPC upgrade.

References

[1] D.R. Nygren and J.N. Marx, *Spectroscopy with multichannel correlation radiometers*, *Phys. Today* **31N10** (1978) 46.

[2] STAR collaboration, K.H. Ackermann et al., *The STAR time projection chamber*, *Nucl. Phys.* **A 661** (1999) 681.

[3] J. Alme, Y. Andres, H. Appelshauser, S. Bablok, N. Bialas et al., *The ALICE TPC, a large 3-dimensional tracking device with fast readout for ultra-high multiplicity events*, *Nucl. Instrum. Meth.* **A 622** (2010) 316 [arXiv:1001.1950].

[4] G. Charpak, R. Bouclier, T. Bressani, J. Favier and C. Zupancic, *The use of multiwire proportional counters to select and localize charged particles*, *Nucl. Instrum. Meth.* **62** (1968) 262.

[5] F. Sauli, *GEM: A new concept for electron amplification in gas detectors*, *Nucl. Instrum. Meth.* **A 386** (1997) 531.

[6] M.C. Altunbas, M. Capeans, K. Dehmelt, J. Ehlers, J. Friedrich et al., *Construction, test and commissioning of the triple-GEM tracking detector for COMPASS*, *Nucl. Instrum. Meth.* **A 490** (2002) 177.

[7] B. Ketzer, Q. Weitzel, S. Paul, F. Sauli and L. Ropelewski, *Performance of triple GEM tracking detectors in the COMPASS experiment*, *Nucl. Instrum. Meth.* **A 535** (2004) 314 [*Erratum ibid.* **A 648** (2011) 293].

[8] B. Ketzer et al. *A triple-GEM detector with pixel readout for high-rate beam tracking in COMPASS*, *NSS IEEE Conf. R.* **1** (2007) 242 Piscataway, NJ, U.S.A.

[9] COMPASS collaboration, P. Abbon et al., *The COMPASS experiment at CERN*, *Nucl. Instrum. Meth.* **A 577** (2007) 455 [hep-ex/0703049].

[10] G. Bencivenni, G. Felici, F. Murtas, P. Valente, W. Bonivento et al., *A triple GEM detector with pad readout for high rate charged particle triggering*, *Nucl. Instrum. Meth.* **A 488** (2002) 493.

[11] Z. Fraenkel, A. Kozlov, M. Naglis, I. Ravinovich, L. Shekhtman et al., *A Hadron blind detector for the PHENIX experiment at RHIC*, *Nucl. Instrum. Meth.* **A 546** (2005) 466 [physics/0502008].

[12] M.G. Bagliesi, M. Berretti, E. Brucken, R. Cecchi, E. David et al., *The TOTEM T2 telescope based on triple-GEM chambers*, *Nucl. Instrum. Meth.* **A 617** (2010) 134.

[13] G. Bencivenni and D. Domenici, *An ultra-light cylindrical GEM detector as inner tracker at KLOE-2*, *Nucl. Instrum. Meth.* **A 581** (2007) 221.

[14] D. Abbaneo et al., *Characterization of GEM detectors for application in the CMS muon detection system*, *NSS/MIC IEEE Conf. R.* (2010) 1416.

[15] S. Bachmann, A. Bressan, M. Capeans, M. Deutel, S. Kappler et al., *Discharge mechanisms and their prevention in the gas electron multiplier (GEM)*, *Nucl. Instrum. Meth.* **A 479** (2002) 294.

[16] M. Killenberg, S. Lotze, J. Mnich, A. Munnich, S. Roth et al., *Charge transfer and charge broadening of GEM structures in high magnetic fields*, *Nucl. Instrum. Meth.* **A 530** (2004) 251.

[17] S. Bachmann, A. Bressan, L. Ropelewski, F. Sauli, A. Sharma et al., *Charge amplification and transfer processes in the gas electron multiplier*, *Nucl. Instrum. Meth.* **A 438** (1999) 376.

[18] A. Breskin, A. Buzulutskov, R. Chechik, B.K. Singh, A. Bondar et al., *Sealed GEM photomultiplier with a CsI photocathode: Ion feedback and ageing*, *Nucl. Instrum. Meth.* **A 478** (2002) 225.

[19] A. Bondar, A. Buzulutskov, L.I. Shekhtman and A. Vasiljev, *Study of ion feedback in multi GEM structures*, *Nucl. Instrum. Meth.* **A 496** (2003) 325 [physics/0208017].

[20] R. Chechik, M. Balcerzyk, A. Breskin, A. Buzulutskov, G.P. Guedes et al., *Progress in GEM-based gaseous photomultipliers*, *Nucl. Instrum. Meth.* **A 502** (2003) 195.

[21] F. Sauli et al., *Electron Collection and Ion Feedback in GEM-Based Detectors*, *IEEE Trans. Nucl. Sci* **50** (2003) 803.

[22] D. Mormann, A. Breskin, R. Chechik and D. Bloch, *Evaluation and reduction of ion back-flow in multi-GEM detectors*, *Nucl. Instrum. Meth.* **A 516** (2004) 315.

[23] R. Veenhof, *Garfield - simulation of gaseous detectors*, http://garfield.web.cern.ch 1984-2010.

[24] F.V. Böhmer, M. Ball, S. Dorheim, C. Höppner, B. Ketzer et al., *Simulation of Space-Charge Effects in an Ungated GEM-based TPC*, *Nucl. Instrum. Meth.* **A 719** (2013) 101 [arXiv:1209.0482].

[25] *ANSYS*. Academic Research, Release 13.0.2012 http://www.ansys.com.

[26] H.W. Ellis, R.Y. Pai and E.W. McDaniel *Transport properties of gaseous ions over a wide energy range*, *Atom. Data Nucl. Data* **17** (1976) 177.

[27] H.W. Ellis and E.W. McDaniel *Transport properties of gaseous ions over a wide energy range. Part II*, *Atom. Data Nucl. Data* **22** (1978) 179.

[28] H.W. Ellis, *Transport properties of gaseous ions over a wide energy range. Part III*, *Atom. Data Nucl. Data* **31** (1984) 113.

[29] A.V. Lyashenko, A. Breskin, R. Chechik, J.M.F. Dos Santos, F.D. Amaro et al., *Efficient ion blocking in gaseous detectors and its application to gas-avalanche photomultipliers sensitive in the visible-light range*, *Nucl. Instrum. Meth.* **A 598** (2009) 116 [arXiv:0804.4396].